

Passively mode-locked interband cascade lasers

Mahmood Bagheri^a, Clifford Frez^a, Igor Vurgaftman^b, Jonas Westberg^c, Lukasz A. Sterczewski^{a,b}, Mathieu Fradet^a, Ivan Grudinin^a, Chadwick L. Canedy^b, William W. Bewley^b, Charles D. Merritt^b, Chul Soo Kim^b, Jerry R. Meyer^b and Gerard Wysocki^c

^aJet Propulsion Laboratory, California Institute of Technology, Pasadena, CA 91109

^bNaval Research Laboratory, Washington, DC 20375, USA

^cDepartment of Electrical Engineering, Princeton University, Princeton N.J. 08544

ABSTRACT

Optical frequency combs have revolutionized the field of high resolution real-time molecular spectroscopy. Here, we demonstrate an electrically-driven optical frequency comb whose sub-picosecond pulses span more than 1 THz of spectral bandwidth centered near 3.3 μm . This is achieved by passively mode locking an interband cascade laser in a multi-contact architecture with gain and saturable absorber sections monolithically integrated on the same chip.

Keywords: mode-locked laser, spectroscopy, semiconductor laser

1. INTRODUCTION

Since their inception, interband cascade lasers (ICLs) have revolutionized mid-infrared laser spectroscopy, as they have made the 3-6 μm wavelength range with many molecular absorption spectral features accessible with unprecedented power efficiency at low drive power.^{1,2} To-date, much attention has been devoted to the development of high spectral purity single mode distributed feedback (DFB) ICLs with high wall plug efficiency for tunable diode laser absorption spectroscopy (TDLAS).^{3,4} However, optical frequency combs have revolutionized the field of high resolution molecular spectroscopy.⁵ Mode-locked interband cascade lasers (ICL) are ideal sources for mid-infrared dual frequency comb spectroscopy due to their compact size, ease of use and high power efficiency.⁶⁻⁸

2. PASSIVELY MODE-LOCKED INTERBAND CASCADE LASERS

2.1 Interband Cascade Lasers

The interband cascade laser (ICL) is a promising mid-infrared (IR) (defined here as $\lambda= 3-6 \mu\text{m}$) source that combines the relatively long upper-level recombination lifetime of a conventional diode laser with the voltage-efficient cascading scheme introduced by the quantum cascade laser ((QCL) which produces coherent light via intersubband transitions within the conduction band. The mid-IR spectral region has gained increasing relevance because it hosts numerous ‘fingerprint’ spectral lines that can be used to sense trace gases such as methane, carbon dioxide, carbon monoxide, formaldehyde, etc. Therefore, ICLs offer a practical realization of sensing systems capable of detection and quantification of such molecules at low power and high sensitivity.

In a conventional diode laser, electrons and holes are injected from opposite sides of a p-n heterojunction, ideally populating all of the multi quantum wells (MQWs) equally. Therefore, the total threshold current density is given by MJ , where J is the threshold current density per QW, and M is the number of QWs. This implies that the parasitic voltage drop proportional to the current scales with the number of QWs. In the mid-IR, the parasitic drop tends to be relatively more significant compared to the ‘useful’ voltage $\hbar\omega/e$, since the currents are often high and the photon energy is smaller at shorter wavelengths.

Cascading mitigates this inefficiency by providing a practical means for connecting the MQWs ‘in series’, i.e. with the same current flowing through every stage and each injected carrier traversing every active QW in turn.⁹

Further author information: (Send correspondence to M.B.)
M.B.: E-mail: mahmood.bagheri@jpl.nasa.gov

Cascading can therefore reduce the net threshold power density considerably, provided the required recycling of carriers from valence to conduction band within each stage does not introduce much additional voltage or current.^{10,11} By exploiting the unusual semi-metallic band alignment between the narrow-gap semiconductors InAs and Ga(In)Sb, the ICL also avoids the appreciable internal optical losses (especially due to free hole absorption) that could potentially occur if every stage incorporated a heavily-doped tunnel junction.¹

In an ICL structure, the active core is comprised of multiple repeated stages, each of which can be subdivided into: (1) the active quantum wells (QWs); (2) the hole injector; and (3) the electron injector. The active QWs can have a type II or type I band alignment. The conduction and valence band profiles in a typical type II ICL designed for emission at $\lambda = 3.7 \mu\text{m}$ are shown in Fig. 1, which includes the ‘W’ active regions for two successive stages. The semi-metallic interface is seen to separate the hole injector, comprised of coupled GaSb/AlSb QWs, from the electron injector consisting of coupled InAs/AlSb QWs. The field-dependent band overlap between states in the hole injector and active hole QW on the one hand, and states in the electron injector and active electron QW in the next stage on the other determines the carrier densities throughout the active core.¹²

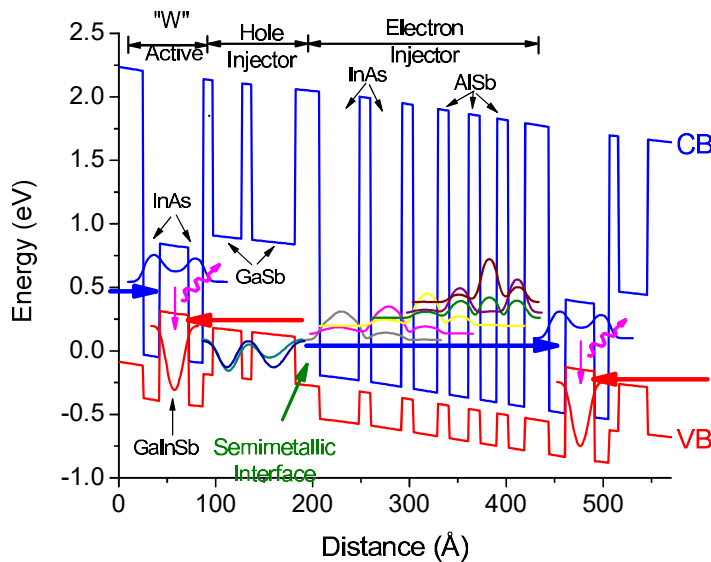


Figure 1. Band diagram of 1.5 stages of a typical ICL active core. Wavefunction probability densities and zone-centre energies (indicated by the wavefunction zero points) for some of the most important subbands are superimposed. The probability densities for the active electron (hole) subbands are indicated with blue (red) lines, while those for the injector-electron (hole) subbands are indicated with wine-coloured (green) lines. The blue (red) arrows indicate the positions of the quasi Fermi levels in each stage.

2.2 Passively Mode-locked lasers

Passive mode locking is induced by incorporating a saturable absorber in the laser cavity. The saturable absorber provides an intensity dependent loss mechanism for which only laser light with an intensity above a threshold is unattenuated, whereas all incident light below that threshold is absorbed. Laser pulses with a higher intensity are thus selectively amplified, a process favoring high bandwidth pulses since they offer the shortest and highest intensity pulses.

Such mode-locked lasers can be formed monolithically in a split-contact gain/saturable-absorber architecture, in which the top contact is divided into a longer, forward-biased gain section and a shorter SA section (Fig. 2).¹³ In the visible and near IR, several variations on this geometry have generated ultra-short (sub-picosecond) transform-limited pulses with high repetition rates (terahertz) and low jitter, for optical communication and other applications.

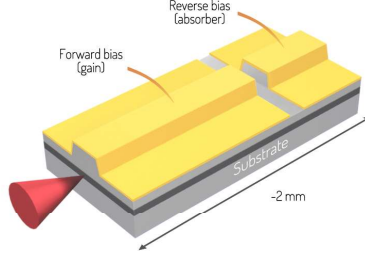


Figure 2. Schematic representation of a passively mode-locked semiconductor laser diode in a split contact architecture.

2.3 Ion Implantation of ICL structures

For this architecture to be effective, the material gain recovery time (τ_g) should exceed the cavity round trip time, τ_{RT} , which is satisfied in an ICL due to the long carrier lifetime for interband transitions ($\tau_g \sim 500$ ps, vs. $\tau_{RT} \sim 100$ ps for a 4 mm long cavity). Furthermore, the time required for the SA section to recover strong absorption (τ_{abs}) should be shorter than the gain recovery time. These conditions open an amplification window around the pulse because rapid absorption recovery shortens its leading edge of the pulse. While the same process can also shorten the trailing edge if τ_{abs} is shorter than the pulse width, the present devices do not fall in the fast SA regime. Several schemes are commonly used to accelerate the absorption recovery in a mode-locked diode laser that monolithically incorporates a saturable absorber. These include ion implantation and the use of a reverse bias on the split contact. In our demonstration, τ_{abs} was reduced by implanting high-energy H^+ ions, and simultaneously a reverse bias was applied to the SA section during operation. The carrier lifetime reduction for ion implanted ICL devices was estimated by comparing the photoluminescence spectrum peak value for a series of ICL PL structures implanted with H^+ ions at 50 KeV and varying ion dosages. It is known that the PL intensity is linearly dependent on the carrier lifetime.¹⁴ Figure 3(a) shows collected photoluminescence spectra

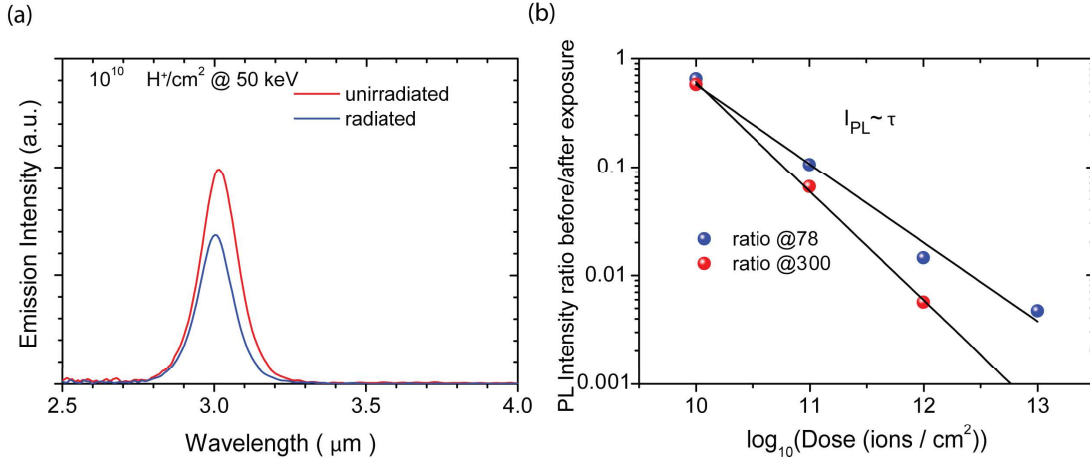


Figure 3. (a) Room temperature photoluminescence spectra collected for a regular IC PL structure (red) and an IC PL structure exposed to $10^{10} H^+ cm^{-2}$. (b) PL intensity ratio for PL structures before and after exposure to H^+ ions at different ion dosages and two different temperatures.

for a regular IC PL structure (red) and one an IC PL structure exposed to $110 H^+ cm^{-2}$ (blue). Figure 3(b) also shows the ratio of the measured photoluminescence before and after irradiation. Figure 3(b) implies that more than 100 times reduction in carrier lifetime can be achieved by exposing the IC PL structures to a $10^{12} H^+ cm^{-2}$ stream of 50 KeV ions.

2.4 Device Fabrication

Using interband-cascade laser structures engineered to emit in the 3-4 μm spectral regime, we modify the waveguide structures by including an ion-implanted section at the end of the 4-mm-long resonator cavity. The laser cavity is sub-divided into two sections, absorber and gain. Using proton-implantation with an optimized dose and concentration, we define the absorber section by contact lithography and masking the remaining surface of the laser wafer with thick electroplated gold approximately several-micrometers-thick. The ion dose and energy for the IC laser structure is then adjusted from the IC PL structure dose and energy experiment described above. It is noted that the implantation depth depends on the laser structure, which is typically greater than 2- μm -deep. After implantation, a lift-off process, leaving alignment marks to indicate implanted regions, removes the gold mask. These alignment marks define the locations of the ridge-waveguide (RWG) and subsequent laser features.

After implantation, the remaining fabrication proceeds according to our standard process. Using contact lithography, a narrow RWG less than 4- μm -wide is etched into the laser wafer to the bottom of the SCL, by a chlorine-based inductively coupled plasma. The RWG is passivated with silicon nitride and a via is patterned by contact lithography on the top of the ridge surface. By electron-beam evaporation, a layer of Au/Ge is deposited into the via and a thick gold pad by electroplating on top of the contact metal for wire-bonding and heat extraction. Both the gain and absorber sections are coated with metal separated by a gap, so that each can be biased individually. To yield mirror-like facets at the ends of the laser cavity, the whole wafer is thinned by mechanical lapping of the substrate to approximately 100- μm -thick. The backside of the wafer is blanket-coated with Au/Ge and then annealed at 260 $^{\circ}\text{C}$ in a reducing environment. The individual laser devices are then cleaved into chips, solder mounted to heat sinks and wire-bonded for performance testing.

3. LASER MODE-LOCKED OPERATION

3.1 Laser output power and optical spectrum

After device fabrication, the lasers are cleaved into laser bars and a high-reflection coating layer is deposited on the back facet. Subsequently, devices are separated into individual laser chips and mounted on a BeO submount for better heat extraction and ease of operation. Figure 4(a) shows an optical image of a mounted device with the front facet highlighted. The devices are positioned on a TEC cooled stage. Lasers are biased by applying current through the longer gain section, while a reverse bias is applied to the SA section through a bias-T. Figure 4(b) shows a schematic of the measurement setup. A calibrated thermopile detector was used to measure the average laser output power. For spectral measurements, the laser emission was collimated using a high numerical aperture lens and directed onto a Fourier transform infra-red (FTIR) spectrum analyzer. Figure 5(a) illustrates

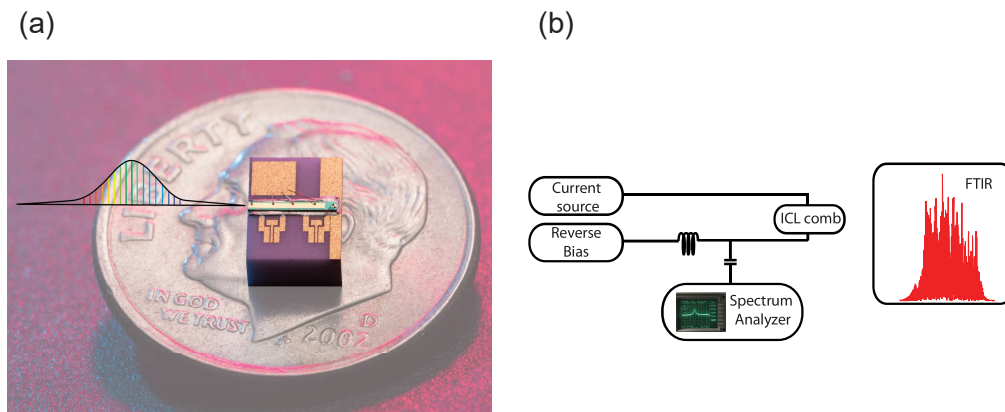


Figure 4. (a) A mode-locked IC laser mounted on a BeO submount (b) Measurement setup layout

the light-current-voltage characteristics of an ICL cavity measured at different heat sink temperatures when the SA contact is short. The laser threshold current density is slightly higher than for state-of-the-art ICLs, because the

SA section introduces additional optical loss into the cavity.³ The laser threshold current increases and the slope efficiency decreases as the reverse bias applied to the SA section increases. This is mainly due to an increase in the laser's optical cavity losses.

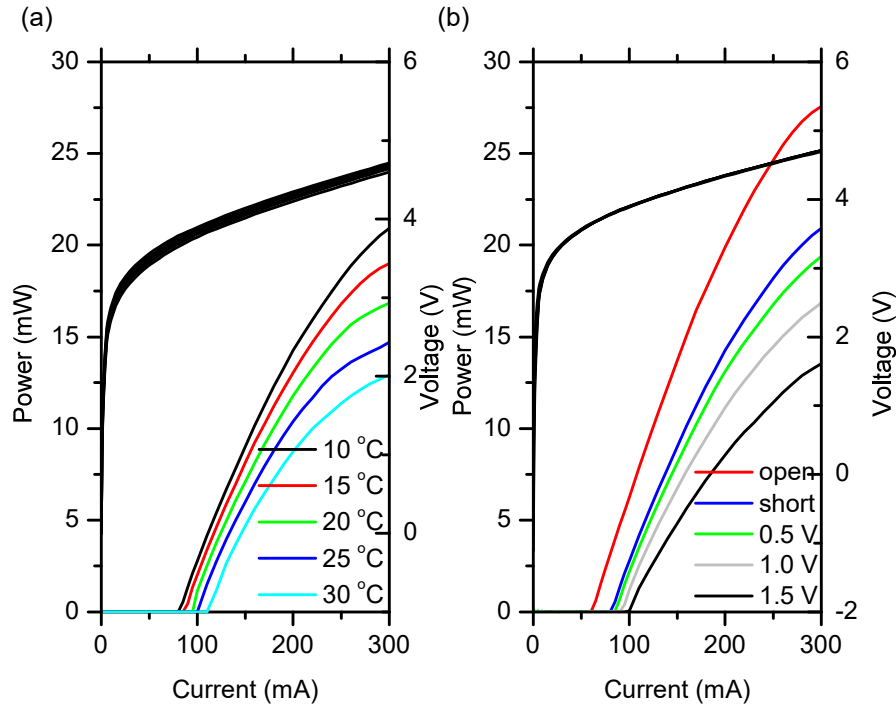


Figure 5. (a) Collected output power (left axis) and bias voltage of the mode-locked ICL vs. current at different heat sink temperatures when the SA section is short. (b) Collected output power (left axis) and bias voltage of the mode-locked ICL vs. current at $T=15^\circ\text{C}$ at different SA section reverse bias values.

Figure 6(a) shows measured optical spectrum of the mode-locked ICL operating at $I=200\text{ mA}$ and $T=15^\circ\text{C}$, with -1.2 V applied to the SA section. The spectrum measured on an FTIR spectrum analyzer. The optical spectrum analyzer demonstrates simultaneous lasing of multiple axial modes of the laser cavity.

In this geometry, the saturable absorber section functions as a fast optical detector that produces an electrical RF tone near the round-trip frequency. This may be used to analyze the laser performance and synchronize external events. Figure 6(b) shows a narrow RF spectrum for the multi-section ICL operating with linewidth only 2.1 KHz . The narrow linewidth, large signal-to-noise ratio, and stability of this beat note confirm that mode locking has been achieved, with negligible random drift of the relative phases of the modes lasing simultaneously in the cavity.

4. SUMMARY

We report the demonstration of an ICL based mode-locked laser operating near the $3.25\text{ }\mu\text{m}$ region. This is an important spectroscopy region where there is a cluster of absorption features of C-H bonds. Our demonstration will enable novel fast and sensitive sensing systems for simultaneous and real-time detection and quantification of multiple molecules.

ACKNOWLEDGMENTS

This work was in part performed at the Jet Propulsion Laboratory (JPL), California Institute of Technology, under contract with the NASA.

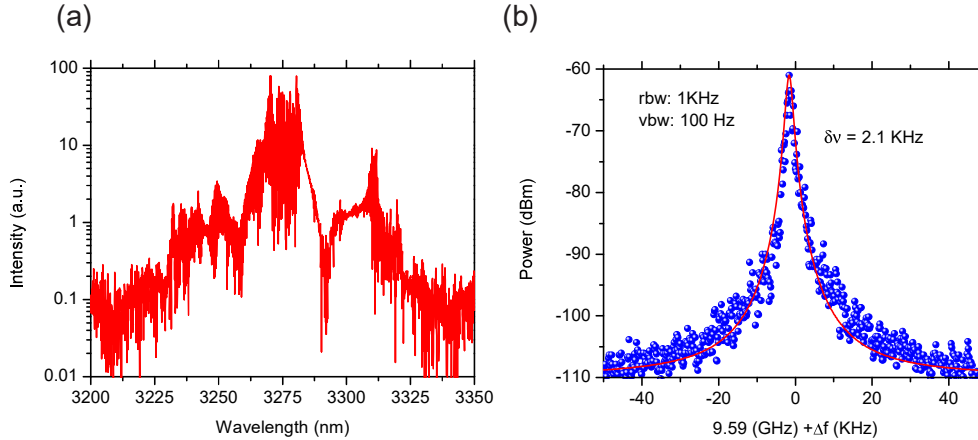


Figure 6. (a) FTIR spectrum of the mode-locked ICL operating at $I = 200$ mA and $T = 15$ ^{circ}C, with the SA junction reverse biased at -1.2 V, (b) RF beat-note with 2.1 KHz linewidth measured under the same operating conditions as (a).

Copyright 2019. All rights reserved.

REFERENCES

- [1] Vurgaftman, I., Bewley, W., Canedy, C., Kim, C., Kim, M., Merritt, C., Abell, J., Lindle, J., and Meyer, J., "Rebalancing of internally generated carriers for mid-infrared interband cascade lasers with very low power consumption," *Nature communications* **2**, 585 (2011).
- [2] Vurgaftman, I., Geiser, P., Bewley, W. W., Merritt, C. D., Canedy, C. L., Warren, M. V., Kim, M., Kim, C. S., and Meyer, J. R., [*Sensitive Chemical Detection with Distributed Feedback Interband Cascade Lasers*], 1–19, John Wiley & Sons, Ltd (2006).
- [3] Forouhar, S., Borgentun, C., Frez, C., Briggs, R. M., Bagheri, M., Canedy, C. L., Kim, C. S., Kim, M., Bewley, W. W., Merritt, C. D., Abell, J., Vurgaftman, I., and Meyer, J. R., "Reliable mid-infrared laterally-coupled distributed-feedback interband cascade lasers," *Applied Physics Letters* **105**(5), 051110 (2014).
- [4] Kim, C. S., Kim, M., Abell, J., Bewley, W. W., Merritt, C. D., Canedy, C. L., Vurgaftman, I., and Meyer, J. R., "Mid-infrared distributed-feedback interband cascade lasers with continuous-wave single-mode emission to 80 °C," *Applied Physics Letters* **101**(6), 061104 (2012).
- [5] Coddington, I., Newbury, N., and Swann, W., "Dual-comb spectroscopy," *Optica* **3**, 414–426 (Apr 2016).
- [6] Bagheri, M., Frez, C., Sterczewski, L. A., Gruidin, I., Fradet, M., Vurgaftman, I., Canedy, C. L., Bewley, W. W., Merritt, C. D., Kim, C. S., Kim, M., and Meyer, J. R., "Passively mode-locked interband cascade optical frequency combs," *Scientific Reports* **8**(1), 3322 (2018).
- [7] Schwarz, B., Hillbrand, J., Beiser, M., Andrews, A. M., Strasser, G., Detz, H., Schade, A., Weih, R., and Höfling, S., "A monolithic frequency comb platform based on interband cascade lasers and detectors," (2018).
- [8] Feng, T., Shterengas, L., Hosoda, T., Belyanin, A., and Kipshidze, G., "Passive mode-locking of 3.25 μ m gasb-based cascade diode lasers," *ACS Photonics* **5**(12), 4978–4985 (2018).
- [9] Yang, R. Q. and Pei, S. S., "Novel type-ii quantum cascade lasers," *Journal of Applied Physics* **79**(11), 8197–8203 (1996).
- [10] Olesberg, J. T. and Flatté, M. E., [*Theory of Mid-wavelength Infrared Laser Active Regions: Intrinsic Properties and Design Strategies*], 3–92, Springer London, London (2006).
- [11] Vurgaftman, I., Bewley, W. W., Canedy, C. L., Kim, C. S., Kim, M., Lindle, J. R., Merritt, C. D., Abell, J., and Meyer, J. R., "Mid-ir type-ii interband cascade lasers," *IEEE Journal of Selected Topics in Quantum Electronics* **17**, 1435–1444 (Sep. 2011).

- [12] Vurgaftman, I., Weih, R., Kamp, M., Meyer, J. R., Canedy, C. L., Kim, C. S., Kim, M., Bewley, W. W., Merritt, C. D., Abell, J., and Höfling, S., “Interband cascade lasers,” *Journal of Physics D Applied Physics* **48**, 123001 (Apr. 2015).
- [13] Avrutin, E. A., Marsh, J. H., and Portnoi, E. L., “Monolithic and multi-gigahertz mode-locked semiconductor lasers: constructions, experiments, models and applications,” *IEE Proceedings - Optoelectronics* **147**, 251–278 (Aug 2000).
- [14] Donetsky, D., Svensson, S. P., Vorobjev, L. E., and Belenky, G., “Carrier lifetime measurements in short-period InAs/GaSb strained-layer superlattice structures,” *Applied Physics Letters* **95**(21), 212104 (2009).